http://dx.doi.org/10.5012/bkcs.2014.35.8.2311

Conformations and Vibrational Frequencies of a Precursor of Benzovesamicol Analogues Studied by Density Functional Theories

Jong-Kil Park and Sang Joon Choe[†,*]

Department of Environmental Engineering, Atmospheric Environment Information Research Center, Inje University, Kimhae 621-749, Korea
[†]*Department of Chemistry, Institute of Basic Science, Inje University, Kimhae 621-749, Korea.* [*]*E-mail: chemcsj@inje.ac.kr*
Received October 4, 2013, Accepted April 17, 2014

Conformations and vibrational frequencies of the racemic (2*RS*,3*RS*)-5-amino-3-(4-phenylpiperazin-1-yl)-1,2,3,4-tetrahydronaphthalen-2-ol-(I) [(2*RS*,3*RS*)-(I)], a precursor of benzovesamicol analogues, have been carried out using various DFT methods (M06-2X, B3LYP, B3PW91, PBEPBE, LSDA, and B3P86) with basis sets of 6-31G(d), 6-31+G(d,p), 6-311+G(d,p), 6-311++G(d,p), cc-pVTZ, and TZVP. The LSDA/6-31G(d) level of theory shows the best performance in reproducing the X-ray powder structure. However, the PBEPBE/cc-pVTZ level of theory is the best method to predict the vibrational frequencies of (2*RS*,3*RS*)-(I). The potential energy surfaces of racemic pairs (2*RS*,3*RS*)-(I) and -(II) are obtained at the LSDA/6-31G(d) level of theory in the gas phase and in water. The results indicate that (2*RS*,3*RS*)-(I) are more stable by ~0.75 kcal/mol in energy than (2*RS*,3*RS*)-(II) in water, whereas conformer AIIg and BIIg are more stable by ~0.04 kcal/mol than AIg in gas phase. In particular, the hydrogen bond distances between the N of piperazine and the OH of tetrahydronaphthalen become longer in gas, compared with those in the water phase. Vibrational frequencies calculated at the PBEPBE/cc-pVTZ level of theory in the gas phase are larger than those in water, whereas their intensities in the gas phase are weaker than those in water.

Key Words : Benzovesamicol analogues, DFT methods, Conformations, Vibrational frequencies, Diagnosis of Alzheimer's disease

Introduction

Racemic (2*RS*,3*RS*)-5-amino-3-(4-phenylpiperazin-1-yl)-1,2,3,4-tetrahydronaphthalen-2-ol-(I) [(2*RS*,3*RS*)-(I)] is a precursor for the preparation of benzovesamicol analogues, which are stereoselective inhibitors of acetylcholine uptake in presynaptic cholinergic vesicles. Benzovesamicol analogues and selected atomic numbers for (2*RS*, 3*RS*)-(I) are shown in Figure 1. Radiolabeled benzovesamicol analogues have been extensively used as imaging probes in single-photon emission computedand positron emission tomography in *in vitro* and *in vivo* studies of Alzheimer's disease.[1-8] Assad *et al.* have recently synthesized (2*RS*,3*RS*)-(I) and analyzed its structure by FT-IR and NMR measurements and X-ray powder diffraction.[9]

DFT has been extensively used to study various aspects of molecules with main group atomic species.[10-16] Approximations in DFT permit the accurate calculation of certain physical quantities. The most widely used approximation in physics is the local-density approximation (LDA). Local spin-density approximation (LSDA) is the straightforward generation of LDA including electron spin. The exchange energy in hybrid methods (*e.g.*, M06-2X, B3LYP, B3PW91, PBEPBE, and B3P86) is combined with the exact energy from Hartree–Fock theory. Adjustable parameters in hybrid functionals are generally fitted to a training set of molecules. Although results obtained from hybrid functionals are usually sufficiently accurate for most applications, a systematic method to improve these functionals has yet to be established and compared with several traditional wave-function-based methods, such as configuration interaction or coupled cluster theory. Thus, calculation errors for the conformational structure and properties of (2*RS*,3*RS*)-(I) should be estimated and compared with other methods or experiments.[9]

Applications of different DFT methods and various basis sets to provide accurate conformations and vibrational frequencies of (2*RS*,3*RS*)-(I) have not been analyzed yet. This study has the following two main objectives: (1) to investigate the performance of different DFT methods and effect of different basis sets on predicting the conformational structures and vibrational spectra of (2*RS*,3*RS*)-(I) in gas phase and water solution, and (2) to study the conformational structures and vibrational spectra of (2*RS*,3*RS*)-(II). This study provides theoretical data and insights into the conformational structure preferences of racemic (2*RS*,3*RS*)-(I).

Computational Methods

All calculations were performed with the Gaussian 09 package.[17] All structures were initially optimized at the HF/6-31G(d) starting the X-ray power structure. The structure of (2*RS*,3*RS*)-(I) were reoptimized and its vibrational frequencies were calculated in the gas phase using various DFT methods, including M06-2X,[18] B3LYP,[19] LSDA,[20] B3PW91,[21] PBEPBE,[22] and B3P86,[23] and different basis sets, including 6-31G(d), 6-31+G(d,p), 6-311+G(d,p), 6-311++G(d,p), cc-

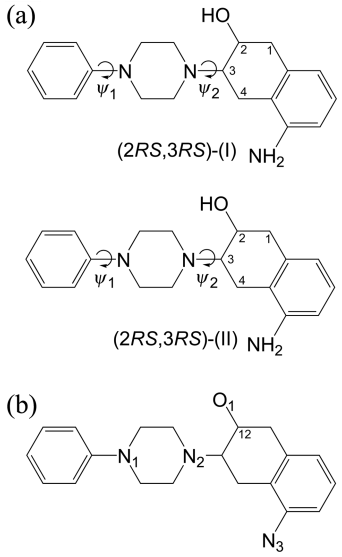

Figure 1. Precusors of benzovesamicol analogues. (a) (2*RS*,3*RS*)-(I) and (2*RS*,3*RS*)-(II) are racemic compounds. Ψ_1 and Ψ_2 are dihedral angles. (b) Selected atomic numbers for (2*RS*,3*RS*)-(I).

pVTZ, and cc-pVQZ. In addition, the potential surfaces of (2*RS*,3*RS*)-(I) and -(II) were obtained at the LSDA/6-31G(d) level of theory in the gas phase and in water. The solvation free energies were calculated using the implicit Solvation Model based on Density (SMD) method.[24] The scale factor used for vibrational frequencies was 0.944.[25]

Results and Discussion

Comparison of Structures Optimized with Different Methods and Various Basis Sets for (2*RS*,3*RS*)-(I). The molecular structure of (2*RS*,3*RS*)-(I) with numerical labels is shown in Figure 1. Table S1 (Supporting Information) provides the comparison of RMSDs between calculated coordinates in the gas phase among different DFT methods at the 6-31G(d) basis set and the X-ray data for (2*RS*,3*RS*)-(I). RMSD can obtain a more accurate conformational structure among all the methods tested.[26] RMSD is the measure of the average distance between the atoms (usually the backbone atoms) of a superimposed 3D structure.

The calculated RMSDs are 2.7793 Å for M06-2X, 2.7923 Å for B3LYP, 2.7777 Å for LSDA, 2.7854 Å for B3PW91, 2.7958 Å for PBEPBE, and 2.7849 Å for B3P86. Thus, of all the methods tested, the LSDA method has the least RMSD between the calculated coordinates of the gas phase and experimental set-up (powder).[9] As shown in Table S1, differences exist between the calculated and X-ray parameters because experimental values were obtained from molecules in solid powder state, whereas theoretical values were based on an isolated molecule in gas phase.

The comparison of RMSDs between calculated coordinates in the gas phase and X-ray data using various basis sets at LSDA calculation for (2*RS*,3*RS*)-(I) is shown in Table S2. The RMSDs are as follows: 2.7777 Å for 6-31G(d), 2.7819 Å for 6-31+G(d, p), 2.7850 Å for 6-311+G(d,p), 2.7853 Å for 6-311++G(d,p), 2.7819 Å for cc-PVTZ, and 2.7822 Å for TZVP. Thus, of all basis sets tested, 6-31G(d) has the least RMSD. However, the RMSDs between the calculated coordinates in the gas phase and X-ray data are significantly high. We compare the selected structural parameters of the X-ray and calculated parameters to identify the reason for the significantly high deviations.

Table 1. Selected Structure Parameters (Å, °) calculated with LSDA/6-31G(d) method for (2*RS*,3*RS*)-(I) and (2*RS*,3*RS*)-(II)

	Exp[a]	(2*RS*,3*RS*)-(I)	(2*RS*,3*RS*)-(II)
C13-C14	1.520(9)	1.498	1.496
C14-C15	1.402(10)	1.398	1.399
C15-C16	1.493(10)	1.497	1.501
C13-C14-C15	120.9(9)	120.8	122.5
C15-C14-C17	123.8(8)	119.7	119.1
C14-C15-C16	122.9(9)	122.5	120.5
C14-C15-C20	113.2(10)	119.6	120.3
C7-N1-C6-C5 (Ψ_1)[c]	-38.1(12)	4.0	6.0
C8-N2-C11-C12 (Ψ_2)[c]	-154.5(5)	-162.0	-156.0
C13-C14-C15-C20	169.3(8)	179.8	-179.2
C17-C14-C15-C16	-174.2(9)	179.1	178.6
O1—H1O[b]…N2	2.33	1.91	1.90

[a]Ref 9. [b]Intramolecular hydrogen bond distance (O1H---N2). [c]See Figure 1.

Selected structural parameters calculated using the LSDA/6-31G(d) method for (2*RS*,3*RS*)-(I) are shown in Table 1. In the comparison of the X-ray-generated structure and the calculated structure, the average error of bond length is approximately 0.61%, the bond angle is approximately 0.37%, and the average absolute dihedral angle is approximately 2.1%. Compared with the dihedral angle ($\Psi_1 = -38.1°$) of X-ray data, the calculated angle ($\Psi_1 = 4°$) of gas phase is significantly different in particular. Thus, conformational energy barrier stability is dependent on Ψ_1, as shown in Figure 2. As expected, the energy surface of conformational structures is stabilized with the formation of an intramolecular hydrogen bond at $\Psi_2 = -156°$ to $-162°$, as shown in Table 2. The dihedral angle (Ψ_1) is defined as almost free rotation without steric hindrance. These results indicate that LSDA is consistent with the X-ray data in terms of predicting the conformational structure of (2*RS*,3*RS*)-(I). In addition, the ability of DFT methods to provide reliable molecular structures for the molecule with the main group atomic species is already well-established and used in the scientific field. However, based on RMSD, the LSDA method is selected for structural calculations in this study.

Potential Surfaces of (2*RS*,3*RS*)-(I). Plots of the two-dimensional (2D) contour map in the variation in relative energy (ΔE in kcal/mol) with y_1 and y_2 for (2*RS*,3*RS*)-(I) are shown in Figure 2. The conformational structures of labeled AIg–DIg conformer are labeled to correspond to the calculated structures of AIg-DIg (Figure 3).

Table 2 lists the molecular dihedral angles and relative energies of benzovesamicol analogues, (2*RS*,3*RS*)-(I) and

Table 2. Molecular dihedral angles, relative energies (*E*rel, Kcal/mol)[a], and hydrogen bond distance[b] of (2*RS*,3*RS*)-(I) and (2*RS*,3*RS*)-(II) optimized at the LSDA/6-31G(d) levels in gas phase and water solution

Conformers (Gas Phase)	Dihedral Angles Ψ_1	Dihedral Angles Ψ_2	ΔE in Kcal/mol Hydrogen Bond	Conformers (Water)	Dihedral Angles Ψ_1	Dihedral Angles Ψ_2	ΔE in Kcal/mol Hydrogen Bond
(2*RS*,3*RS*)-(I)				(2*RS*,3*RS*)-(I)			
AIg	4	-162	0.00[a] (1.92)[b]	AIs	-18	-163	0.00[a] (1.88)[b]
BIg	-174	-161	0.00[a] (1.92)[b]	BIs	40	-160	0.12[a] (1.85)[b]
CIg	-168	-168	0.32[a] (1.93)[b]	CIs	136	-166	0.26[a] (1.88)[b]
DIg	-156	-156	0.39[a] (1.92)[b]				
(2*RS*,3*RS*)-(II)				(2*RS*,3*RS*)-(II)			
AIIg	6	-156	-0.04[a] (1.91)[b]	AIIs	11	-166	0.27[a] (1.90)[b]
BIIg	-40	-160	-0.02[a] (1.92)[b]	BIIs	167	-167	0.28[a] (1.90)[b]
CIIg	-155	-155	0.30[a] (1.92)[b]	CIIs	4	-154	0.75[a] (1.85)[b]

[a]Relative energies (ΔE) in Kcal/mol specify differences in total energy (see Table S3 of Supporting Information). Minus sign represents more stable. [b]Intramolecular hydrogen bond between a hydroxyl H atom and an N_2 atom of the piperazine ring (O1-H1O…N2) (see Figure 2)

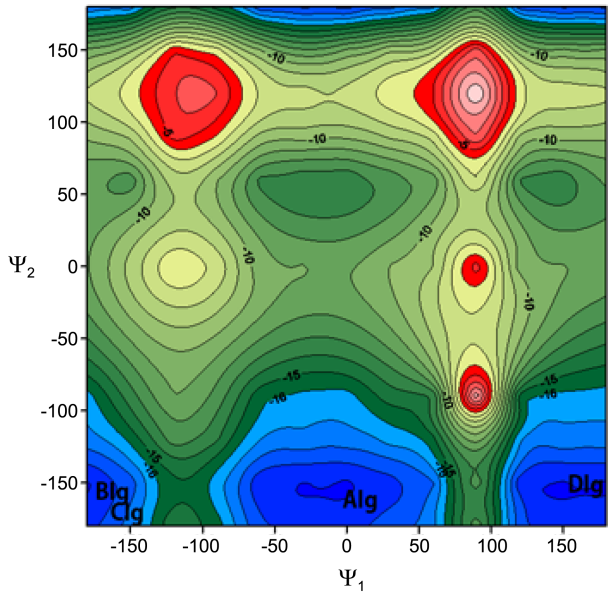

Figure 2. Plots of the 2D contour map in the variation in relative energy (ΔE in kcal/mol) with Ψ_1 and Ψ_2 for (2*RS*,3*RS*)-(I). The structures of labeled AIg-DIg conformers are labeled to correspond to calculated structures of AIg-DIg.

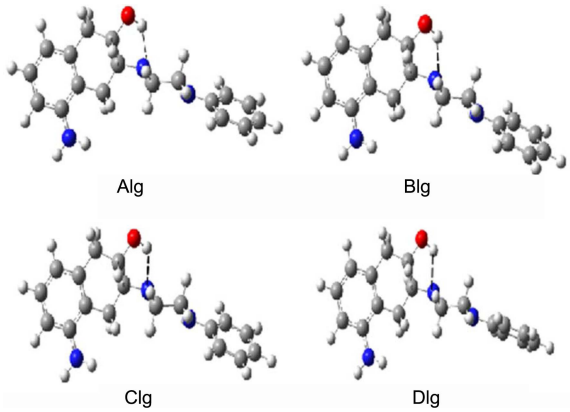

Figure 3. Preferred conformations AIg, BIg, CIg, and DIg of (2*RS*,3*RS*)-(I) at the LSDA/6-31G(d) level of theory in the gas phase. Intramolecular hydrogen bonds are represented by a dashed line. The distances of hydrogen bond for AIg, BIg, and DIg are 1.92 Å and CIg is 1.93 Å.

(2*RS*,3*RS*)-(II), optimized at LSDA/6-31G(d) levels in gas phase and water solution. The conformational structures and relative energies of local minima are almost similar. Although Ψ_1 of conformers significantly differ in dihedral angles, Ψ_2 angles resulting from intramolecular hydrogen bonds have similar angles. The conformational structure stability of (2*RS*,3*RS*)-(I) by the relative energies (ΔE) in gas phase is calculated. ΔE specifies differences in total energy (Table S3), and is expressed as kcal/mol with respect to the stable conformational structure. The lowest relative energy conformation is AIg with intramolecular hydrogen bond between a hydroxyl H atom and an N_2 atom of the piperazine ring (O1-H1O…N2) in Figure 1. The hydrogen bond functions in determining the lowest energy conformation for benzovesamicol analogue structures. The distances of the hydrogen bond for (2*RS*,3*RS*)-(I) are calculated as 1.92 and 1.93 Å. All ΔE values computed with the LSDA/6-31G(d) method, using either one of the optimized conformers, differ by ~0.39 kcal/mol in (2*RS*,3*RS*)-(I) in gas phase.

The energies of conformers at (2*RS*,3*RS*)-(II) are lower than those at (2*RS*,3*RS*)-(I). Thus, the conformers of (2*RS*,3*RS*)-(II) are more stable than those of (2*RS*,3*RS*)-(I). Figure S1 shows the preferred structures AIIg, BIIg, and CIIg of (2*RS*,3*RS*)-(II) at the LSDA/6-31G(d) level in gas phase. The distances of hydrogen bonds are 1.91 and 1.92 Å. All ΔE values computed with the LSDA/6-31G(d) method are shown in Table 2. The conformer AIIg and BIIg are more stable than AIg in gas phase.

The conformational structure stabilities of (2*RS*,3*RS*)-(I) and (2*RS*,3*RS*)-(II) by relative energies in water solution are calculated. The lowest relative energy conformer is AIs. Either one of the optimized conformers differ by ~0.75 kcal/mol in water solution. Compared with gas phase, the hydro-

Table 3. Comparison of vibrational frequencies (in nm) calculated with various DFT methods at 6-31G(d) basis set for (2*RS*,3*RS*)-(I) in gas phase

Exp (cm^{-1})[a]	M062-2X	B3LYP	LSDA	B3PW91	PBEPBE	B3P86
3460 (OH)	3681	3596	3303	3600	3399	3592
3275 ± 75 (NH_2)	3577	3577	3485	3568	3458	3570
3050 (CH=CH, Ar)	3239	3202	3121	3211	3117	3216
2885 ± 34 (CH_2, aliphatic)	3128	3029	2946	3042	2959	3044
2851 (CH_2-NH_2)	3021	2974	2888	2982	2975	2985
1637 (C=C)	1565	1665	1645	1677	1622	1681
1138 (C-N, Piperazine)	1293	1190	1157	1128	1133	1178

[a]Ref. 9

Table 4. Comparison of vibrational frequencies (cm^{-1}) calculated with PBEPBE at different basis sets for (2*RS*,3*RS*)-(I) in gas phase

	PBEPBE				
Exp[a]	6-31+ G(d,p)	6-311+ G(d,p)	6-311++G(d,p)	cc-PVTZ	TZVP
3460 (OH)	3484	3498	3497	3488	3472
3275 ± 75 (NH_2)	3489	3482	3482	3472	2479
3050 (CH=CH, Ar)	3100	3086	3086	3084	3089
2885 ± 34 (CH_2, aliphatic)	2868	2858	2858	2908	2859
2851 (CH_2–NH_2)	2872	2858	2858	2853	2860
1637 (C=C)	1608	1601	1601	1602	1601
1138 (C-N, Piperazine)	1145	1142	1142	1140	1123

[a]Ref. 9

gen bond distances decrease in water solution. Figure S2 shows the preferred conformational structures AIs, BIs, and CIs of (2*RS*,3*RS*)-(I) at the LSDA/6-31G(d) level in water solution. The distances of hydrogen bonds for AIs, BIs, and CIs are 1.88 Å but 1.85 Å for BIs. (2*RS*,3*RS*)-(II) exhibits the structures of AIIs, BIIs, and CIIs in water. The hydrogen bond distances of AIIs and BIIS are 1.90 Å, but CIIs have hydrogen bond distances of 1.85 Å.

Comparison of Vibrational Frequencies Calculated with Different Methods and Basis Sets for (2*RS*,3*RS*)-(I). Table 3 shows the calculated results of vibrational frequencies with different DFT methods at 6-31G(d) basis set for (2*RS*,3*RS*)-(I). Table S4 shows a comparison of mean absolute deviation (MAD, cm^{-1}) between calculated vibrational frequencies and experimental values using various DFT methods at 6-31G(d) basis set for (2*RS*,3*RS*)-(I). The MAD values are as follows: 193.1 cm^{-1} for M06-2X, 133.8 cm^{-1} for B3LYP, 80.4 cm^{-1} for LSDA, 133.1 cm^{-1} for B3PW91, 75.6 cm^{-1} for PBEPBE, and 138.6 cm^{-1} for B3P86.

The simulation spectra of (2*RS*,3*RS*)-(I) are shown in Figures S3 and S4. PBEPBE method has the least MAD between calculated and experimental values, and the deviation error is 2.89%. Thus, PBEPBE is selected for the vibrational frequency calculations. The DFT calculation is desirable for resolving disputes in vibrational assignments, and provides valuable insight for understanding the observed spectral features.

Table 4 shows the calculated results of vibrational frequencies with PBEPBE at different basis set for (2*RS*,3*RS*)-(I). Table S5 shows the comparison of MAD between calculated vibrational frequencies and experimental values using various basis sets for (2*RS*,3*RS*)-(I) by PBEPBE method. The MAD values are as follows: 51.7 cm^{-1} for 6-31+G(d,p), 50.7 cm^{-1} for 6-311+G(d,p), 50.6 cm^{-1} for 6-311++G(d,p), 45.9 cm^{-1} for cc-PVTZ, and 122.6 cm^{-1} for TZVP. MAD of cc-PVTZ basis set is the lowest at 45.9 cm^{-1}, and the deviation

Table 5. Vibrational frequencies (cm^{-1}) of (2*RS*,3*RS*)-(I) and (2*RS*,3*RS*)-(II) calculated at PBEPBE/cc-PVTZ level in gas phase and water solution

Exp	Gas Phase		Water Solution		Type of Vibration
	(2*RS*,3*RS*)-(I)	(2*RS*,3*RS*)-(II)	(2*RS*,3*RS*)-(I)	(2*RS*,3*RS*)-(II)	
3460 (OH)	3488	3479	3308	3433	Stretch
3275 ± 75 (NH_2)	3472	3477	3377	3459	Symmetry Stretch
3050 (CH=CH, Ar)	3084	3115	3036	3090	Stretch
2885 ± 34 (CH_2, aliphatic)	2908	2925	2861	2931	Symmetry Stretch
2851 (CH_2-NH_2)	2853	2869	2815	2890	Stretch
1637 (C=C)	1602	1603	1542	1565	Stretch
1138 (C-N, Piperazine)	1140	1140	1115	1125	Stretch

[a]Ref. 9

error is 1.59%. Thus, PBEPBE/cc-PVTZ is selected for vibrational frequency calculation. The simulation spectra of (2*RS*,3*RS*)-(I) are shown in Figure S5. These results indicate that PBEPBE/cc-PVTZ is consistent with available experimental vibrational frequencies.[9]

Analysis of Vibrational Frequencies for (2*RS*,3*RS*)-(I) and (2*RS*,3*RS*)-(II). Table 5 shows the vibrational frequencies of benzovesamicol analogues, (2*RS*,3*RS*)-(I) and (2*RS*, 3*RS*)-(II), calculated at PBEPBE/cc-PVTZ level in gas phase and water solution. The frequency of the OH stretching region is 3488 cm^{-1} for (2*RS*,3*RS*)-(I) and 3479 cm^{-1} for (2*RS*,3*RS*)-(II) in gas phase. In (2*RS*,3*RS*)-(I), the stretching regions of (CH=CH, Ar), (CH_2-NH_2), (C=C), and (C-N, Piperazine) are 3084, 2853, 1602, and 1140 cm^{-1}, respectively. The symmetry stretch values of (NH_2) and (CH_2, aliphatic) are 3472 and 2908 cm^{-1}, respectively. In (2RS, 3RS)-(II), the stretch values of (CH=CH, Ar), (CH_2-NH_2), (C=C), and (C-N, Piperazine) are 3115, 2869, 1603, and 1140 cm^{-1}, respectively. The symmetry stretch values of (NH_2) and (CH_2, aliphatic) are 3477 and 2925 cm^{-1}, respectively. The frequencies of (2*RS*,3*RS*)-(II) slightly increase than those of (2*RS*,3*RS*)-(I), except for the OH frequency and (C-N, Piperazine). For water solution, the stretch values of (OH), (CH=CH, Ar), (CH_2-NH_2), (C=C), and (C-N, Piperazine) are 3308, 3036, 2815, 1542, and 1115 cm^{-1} in (2*RS*,3*RS*)-(I), respectively. The symmetry stretch values of (NH_2) and (CH_2, aliphatic) are 3377 and 2861 cm^{-1}, respectively. In (2*RS*,3*RS*)-(II), the stretch values of (OH), (CH=CH, Ar), (CH_2-NH_2), (C=C), and (C-N, Piperazine) are 3433, 3090, 2890, 1565, and 1125 cm^{-1}, respectively. The symmetry stretch values of (NH_2) and (CH_2, aliphatic) are 3459 and 2931 cm^{-1}, respectively. The frequencies of gas phase are higher than those of water solution because of the polar solvent effect, whereas the intensities of gas phase are weaker than those of water solution in (2*RS*,3*RS*)-(I). The simulation spectra of (2*RS*,3*RS*)-(I) and (2*RS*,3*RS*)-(II) in gas phase and water solution are shown in Figure S6. In (2*RS*,3*RS*)-(II), the frequencies of (CH_2, aliphatic) and (CH_2-NH_2) in gas phase are lower than those of water solution.

Conclusion

The main findings of this study are summarized as follows:

a) The LSDA/6-31G(d) level is consistent with the results from X-ray crystallography in predicting the conformational structure of racemic pairs (2*RS*,3*RS*)-(I) and (2*RS*,3*RS*)-(II), whereas the PBEPBE/cc-PVTZ level is consistent with the vibrational frequencies.

b) Compared with calculated structures, bond lengths and bond angles are consistent in X-ray-generated structures, except dihedral angles.

c) Dihedral angle (ψ_1) is highly different between calculated gas phase (4°) and X-ray data (–38.1°). Thus, the dihedral angle (ψ_1) is defined as almost free rotation without steric hindrance.

d) (2*RS*,3*RS*)-(I) are more stable than (2*RS*,3*RS*)-(II) in water, whereas conformer AIIg and BIIg are more stable than conformer AIg in gas phase.

e) The hydrogen bond distances become longer in gas, compared with those in water.

f) The frequencies of gas phase are higher than those of water solution because of the polar solvent effect, whereas the intensities of gas phase are weaker than those of water solution for (2*RS*,3*RS*)-(I).

Supporting Information Available. Supporting information includes RMSD lists between calculated coordinates in gas phase and experiment using different DFT methods and various basis sets for (2*RS*,3*RS*)-(I). Molecular dihedral angles and total energies of (2*RS*,3*RS*) and (2*RS*,3*RS*)-(II) are shown in Table S3. MAD values between calculated vibrational frequencies and experimental frequencies are given in Tables S4 and S5. Preferred conformational structures and calculated IR spectra are shown in Figures S1–S5. This

material is available free of charge.

Acknowledgments. This work was supported by the National Research Foundation of Korea (NRF) grant funted by the Korea government (MSIP) (2013-065891).

References

1. Alfonso, A.; Grundahl, K.; Duerr, J. S.; Han, H. P.; Rand, J. B. *Science* **1993**, *261*, 617-619.
2. Auld, D. S.; Kornecook, T. J.; Bastianetto, S.; Quirion, R. *Prog. Neurobiol*. **2002**, *68*, 209-245.
3. Efange, S. M. N.; Garland, E.; Staley, J. K.; Khare, A. B.; Mash, D. C. *Neurobiol. Aging* **1997**, *18*, 407-413.
4. Mulholland, G. K.; Jung, Y. W. *J. Labelled Comp. Radiopharm*. **1992**, *31*, 253-259.
5. Mulholland, G. K.; Jung, Y. W.; Wieland, D. M.; Kilbourn, M. R.; Kuhl, D. E. *J. Labelled Comp. Radiopharm*. **1993**, *33*, 583-591.
6. Nicolas, G.; Patrick, E.; Roger, R. F.; David, J. H.; Sylvie, C.; Lucette, G.; Peter, R.; Stefan, E.; Sylvie, B.; Michael, J. F.; Denis, G.; Michael, K. *Synapse* **2007**, *61*, 962-979.
7. Rogers, G. A.; Parsons, S. M.; Anderson, D. C.; Nilsson, L. M.; Bahr, B. A.; Kornreich, W. D.; Kaufman, B. *J. Med. Chem*. **1989**, *32*, 1217-1230.
8. Zea-Ponnce, Y.; Mavel, S.; Assaad, T.; Kruse, S. E.; Parson, S. M.; Emond, P.; Chalon, S.; Kruse, S.; Giboureau, N.; Kassiou, M.; Guilloteau, D. *Bioorg. Med. Chem.* **2005**, *13*, 745-753.
9. Assad, T.; Rukiah, M. *Acta Cryst*. **2011**, *C67*, o378-o381.
10. Park, J. K.; Choe, S. J. *J. Porphyrins Phthalocyanines* **2013**, *17*, 376-383.
11. Choe, S. J. *Bull. Korean Chem. Soc.* **2012**, *33*, 2861-2866.
12. Choe, S. J.; Shim, Y. K.; Galindev, O. *J. Porphyrins Phthalocyanines* **2012**, *16*, 218-226.
13. Camacho, C.; Cheng, C.; Witek, H. A.; Lee, Y. P. *J. Phys. Chem. A* **2010**, *114*, 11008-11016.
14. Gao, H.; Wei, X.; Liu, X.; Yan, T. *J. Phys. Chem. B* **2010**, *114*, 4056-4062.
15. Zakharov, A. V.; Girichev, G. V. *J. Mol. Struct. (Theochem)* **2008**, *851*, 183-196.
16. Gao, H.; Yan, T.; Zhang, C.; He, H. *Mol. Struct. (Theochem)* **2008**, *857*, 38-43.
17. Frisch, M. J.; Trucks, G. W.; Schlegel, H. B.; Scuseria, G. E.; Robb, M. A.; Cheeseman, J. R.; Scalmani, G.; Barone, V.; Mennucci, B.; Peterson, G. A.; Nakatsuji, H.; Caricato, M.; Hratchian, H. P.; Izmaylov, A. F.; Bloino, J.; Zheng, G.; Sonnenberg, J. L.; Hada, M.; Ehara, M.; Toyota, K.; Fukuda, R.; Hasegawa, J.; Ishida, M.; Nakajima, T.; Hona, Y.; Kitao, O.; Nakai, H.; Vreven, T.; Montgomery, J. A., Jr.; Peralta, J. E.; Ogliaro, F.; Bearpark, M.; Heyd, J. J.; Brothers, E.; Kudin, K. N.; Staroverov, V. N.; Kobayashi, R.; Normand, J.; Raghavachari, K.; Rendell, A.; Burant, J. C.; Lyengar, S. S.; Tomasi, J.; Cossi, M.; Rega, N.; Millam, J. M.; Klene, M.; Knox, J. E.; Cross, J. B.; Bakken, V.; Adamo, C.; Jaramillo, J.; Gomperts, R.; Stratmann, R. E.; Yazyev, O.; Austin, A. J.; Cammi, R.; Pomelli, C.; Ochterski, J. W.; Martin, R. L.; Morokuma, K.; Zakrzewski, V. G.; Voth, G. A.; Salvador, P.; Dnnenberg, J. J.; Dapprich, S.; Daniels, A. D.; Farkas, O.; Foresman, J. B.; Oritz, J. V.; Cioslowski, J.; Fox, D. J.; Gaussian Inc.: Wallingford, CT, 2009.
18. Zaho, Y.; Truhlar, D. G. *J. Phys. Chem*. **2006**, *110*, 5121-5129.
19. Becke, A. D. *J. Chem. Phys*. **1993**, *98*, 5648-5652. *J. Chem. Phys*. **1996**, *104*, 1040-1046. *J. Chem. Phys*. **1997**, *107*, 8554-8560.
20. Vosko, S. H.; Wilk, L.; Nusair, M. *Can. J. Phys*. **1980**, *58*, 1200-1211.
21. (a) Perdew, J. P.; Chevary, J. A.; Vosko, S. H.; Jackson, K. A.; Pederson, M. R.; Singh, D. J.; Fiolhais, C. *Phys. Rev. B* **1992**, *B46*, 6671-6687. (b) Perdew, J. P.; Burk, K.; Wang, Y. *Phys. Rev. B* **1996**, *54*, 16533-16539.
22. Perdew, J. P.; Burk, K.; Ernzerhof, M. *Phys. Rev. Lett*. **1996**, *77*, 3865-3868. *Phy. Rev. Lett.* **1997**, *78*, 1396-1396.
23. Perdew, J. P. *Phy. Rev. B* **1986**, *33*, 8822-8824.
24. Marenich, A. V.; Gramer, C. J.; Truhlar, D. G. *J. Phys. Chem. B* **2009**, *113*, 6378-6396.
25. Merrick, J. P.; Moran, D.; Radom, L. *J. Phy. Chem. A* **2007**, *111*, 11683-11700.
26. Maiorov, V. N.; Grippen, G. M. *J. Mol. Biol*. **1994**, *235*, 625-634.